
A Sketch-and-Project Analysis of Subsampled Natural Gradient Algorithms

Gil Goldshlager¹ Jiang Hu² Lin Lin^{1,3}

Abstract

Subsampled natural gradient descent (SNG) has been used to enable high-precision scientific machine learning, but standard analyses based on stochastic preconditioning fail to provide insight into realistic small-sample settings. We overcome this limitation by instead analyzing SNG as a sketch-and-project method. Motivated by this lens, we discard the usual theoretical proxy which decouples gradients and preconditioners using two independent mini-batches, and we replace it with a new proxy based on squared volume sampling. Under this new proxy we show that the expectation of the SNG direction becomes equal to a preconditioned gradient descent step even in the presence of coupling, leading to (i) global convergence guarantees when using a single mini-batch of any size, and (ii) an explicit characterization of the convergence rate in terms of quantities related to the sketch-and-project structure. These findings in turn yield new insights into small-sample settings, for example by suggesting that the advantage of SNG over SGD is that it can more effectively exploit spectral decay in the model Jacobian. We also extend these ideas to explain a popular structured momentum scheme for SNG, known as SPRING, by showing that it arises naturally from accelerated sketch-and-project methods.

1. Introduction

Neural networks are increasingly gaining traction as an alternative to traditional numerical solvers, with applications including neural network wavefunctions (NNWs, Carleo & Troyer, 2017) and physics-informed neural networks (PINNs, Raissi et al., 2019). For such scientific machine learning problems, precision is prioritized over generalization performance. As a result, natural gradient algorithms

can dramatically outperform more standard machine learning optimizers such as gradient descent and Adam (Pfau et al., 2020; Schätzle et al., 2023; Lin et al., 2023; Müller & Zeinhofer, 2023; Dangel et al., 2024). Furthermore, high iteration costs can be mitigated by *subsampling* (Ren & Goldfarb, 2019), leading to efficient subsampled natural gradient (SNG) algorithms that scale to millions of parameters without approximation. This approach was introduced to the NNW community by (Chen & Heyl, 2024) and since this seminal work, SNG has become a workhorse algorithm for NNWs; see (Rende et al., 2024; Lange et al., 2025; Vecsei & Lado, 2025; Sinibaldi et al., 2025; Misery et al., 2025) and many more. SNG has also demonstrated promising results for PINNs (Schwencke & Furtlehner; Guzmán-Cordero et al., 2025; Jnini & Vella, 2025), though has not yet been widely adopted.

Despite these developments, subsampled natural gradient algorithms remain poorly understood. Analytically, the key challenge lies in controlling the expectation of an optimization step involving a stochastic gradient that is coupled to the inverse of a stochastic preconditioner. The standard way to address this problem is to introduce a theoretical proxy which breaks the coupling using two independent mini-batches. This approach can lead to detailed convergence rates when the sample size is large enough to accurately estimate the preconditioner, but for smaller sample sizes it produces only generic global convergence guarantees (Ren & Goldfarb, 2019; Roosta-Khorasani & Mahoney, 2019; Bollapragada et al., 2019; Martens, 2020; Yang et al., 2020; Wu et al., 2024). As a result, such analyses fail to provide insight into realistic settings in which the sample size is orders of magnitude smaller than the number of parameters. Moreover, this failure is predictable: for such sample sizes the stochastic preconditioner captures only a tiny subset of the parameter space, making it unlikely to be informative for an independently estimated gradient. As a result, even for very simple problems the two mini-batch proxy can exhibit drastically different behavior than the realistic, single mini-batch algorithm; see Figures 2 and 6.

Several recent works have hinted at a different perspective (Chen & Heyl, 2024; Schwencke & Furtlehner; Goldshlager et al., 2024; 2025). These works have viewed the SNG update as the minimal-norm solution to a subsampled linear system rather than an estimator for the deterministic natural

¹Department of Mathematics, University of California, Berkeley
²Yau Mathematical Sciences Center, Tsinghua University
³Lawrence Berkeley National Laboratory. Correspondence to: Gil Goldshlager <ggoldsh@berkeley.edu>.

Conceptual lens	Global guarantees?	Small-Sample Insights?	Principled acceleration?	Technical assumption
Stochastic preconditioning	✓	✗	✗	Two independent mini-batches
Sketch-and-project	✓	✓	✓	Squared volume sampling

Figure 1. Summary of technical contributions relative to previous analyses based on stochastic preconditioning.

gradient direction. Along these lines connections have been drawn to randomized block Kaczmarz methods, which are a special case of the sketch-and-project framework of (Gower & Richtárik, 2015). This direction is promising since sketch-and-project methods use a single sketching matrix for each iteration and admit detailed convergence rates for arbitrary sketch sizes. Nonetheless, it has remained unclear whether this approach can lead to new theoretical insights, particularly since embracing the sketch-and-project perspective requires avoiding the decoupling tactic that has facilitated previous analyses.

2. Contributions

We develop the sketch-and-project approach into a systematic framework for analyzing subsampled natural gradient algorithms. Our starting point is the general parametric optimization problem

$$\min_{\theta} \mathcal{L}(v_{\theta}) \quad (1)$$

where $\theta \in \mathbb{R}^n$ are the parameters, v_{θ} is an element of a function space \mathcal{H} (which we take to be a Hilbert space), and $\mathcal{L} : \mathcal{H} \rightarrow \mathbb{R}$ is a loss defined on the function space. For scientific machine learning the underlying science problem is here represented by $\min_v \mathcal{L}(v)$, while the neural network ansatz is represented by v_{θ} .

In this setting, the availability of high-precision solutions depends on the consistency of the problem, with exact consistency ($v_{\theta^*} = \arg \min_v \mathcal{L}(v)$) enabling exact solutions and approximate consistency ($v_{\theta^*} \approx \arg \min_v \mathcal{L}(v)$) enabling approximate solutions. To understand the effectiveness of SNG for high-precision scientific machine learning, it is thus natural to study its local convergence properties for consistent problems. To do so cleanly, we note that near the minimizer, any consistent parametric optimization problem is approximated to second order as $\mathcal{L}(v_{\theta}) \approx \tilde{\mathcal{L}}(\tilde{v}_{\theta})$, where $\tilde{\mathcal{L}}$ is a quadratic approximation to \mathcal{L} about θ^* and \tilde{v} is a linearization of v about θ^* . Motivated by this fact we focus our convergence rate analysis on the resulting model problem:

Problem 2.1 (Linear least-quadratics). *Let $\mathcal{H} = \mathbb{R}^m$ and*

$$v_{\theta} = J\theta, \quad \mathcal{L}(v) = \frac{1}{2}v^{\top}Hv - v^{\top}b \quad (2)$$

with $H \succ 0$. Then minimize $\mathcal{L}(v_{\theta})$ as in (1).

We call this problem *linear least-quadratics* (LLQ) since it uses a linear ansatz to minimize a quadratic loss function, and we note that the standard linear least-squares is recovered by setting $H = I$. With this context in mind we summarize our contributions as follows:

- We provide an approach to analyzing SNG without decoupling the gradient and the preconditioner.** In particular, we show that under a sampling strategy known as *squared volume sampling* (SVS), the expected SNG direction becomes equal to a preconditioned gradient descent step, even in the presence of coupling (Lemma 4.1). This leads to global convergence guarantees when using a single mini-batch of any size to inform each step (Theorem 4.2), and it establishes SVS-SNG as a new theoretical proxy for SNG. The relevance of this construction is supported by numerical experiments which show that SVS-SNG can be a more faithful proxy for realistic SNG algorithms than previous proxies based on independent mini-batches (Figures 2 and 6).
- We show that the convergence rate of SNG can be controlled by its sketch-and-project structure.** In particular, under SVS we prove an explicit convergence rate for SNG in the linear least-quadratics setting (Theorem 5.1). The results show that as the sample size is varied, the optimal convergence rate scales as α/γ , where α is the standard sketch-and-project convergence rate and γ is a new quantity related to the second moment of the sketch-and-project step. The appearance of α suggests that the advantage of SNG over SGD is that it can more effectively exploit spectral decay in the model Jacobian, which is confirmed empirically in Figure 4. Regarding γ , we provide a preliminary characterization (Proposition 5.3) and numerical evi-

dence which suggests benign behavior (Figure 3), and we defer a thorough analysis to future works.

3. **We extend these ideas to explain a popular structured momentum scheme for SNG.** In particular, we show that the subsampled projected-increment natural gradient (SPRING) algorithm of (Goldshlager et al., 2024) arises naturally from the application of accelerated sketch-and-project methods (Theorem 6.1). This suggests that the advantage of SPRING over SNG should be greatest when the underlying sketch-and-project steps converge slowly, such as when the sample size is small; this phenomenon is confirmed empirically in Figure 5.

Overall, our results suggest that when using subsampled natural gradient algorithms to solve scientific machine learning problems, more attention should be paid to the sketch-and-project properties such as α and γ , and less to the statistical estimation properties such as the variance of the gradient and preconditioner estimates. We note that our results also apply to subsampled Gauss-Newton algorithms for nonlinear least-squares problems, since these are recovered by setting $\mathcal{L}(v) = \frac{1}{2}\|v - b\|^2$. We also note that our results assume $\mathcal{H} = \mathbb{R}^m$, though we see no fundamental barrier to treating infinite dimensional Hilbert spaces with suitable generalizations of squared volume sampling.

3. Background

Recall that our formal starting point is the parametric optimization problem (1). To see the relevance of this problem, note that for NNWs we can set $v_\theta = \Psi_\theta / \|\Psi_\theta\|$ to be the normalized wavefunction and $\mathcal{L}(v) = \langle v, H v \rangle$ to be the expectation value of the energy with respect to the Hamiltonian H . Stochastic minimization of the composite loss function $\mathcal{L}(v_\theta)$ then recovers the variational Monte Carlo method for finding ground states of quantum systems (Foulkes et al., 2001). Common PINN loss functions can also be written in the form of (1); see (Müller & Zeinhofer, 2023; 2024) for relevant treatments.

3.1. Natural Gradient Descent

From a geometric perspective, the intuition behind natural gradient descent is to mimic gradient descent in the function space (Müller & Zeinhofer, 2024). To describe this process we focus in on a single iteration denoted by index t and parameters θ_t , and we define the *function space gradient* $r = \nabla_v \mathcal{L}(v_{\theta_t}) \in \mathcal{H}$ and the *model Jacobian* $J = \nabla_\theta v_{\theta_t} : \mathbb{R}^n \rightarrow \mathcal{H}$. Here r can be the standard L^2 gradient or, for applications such as NNWs when the model v_θ is restricted to a manifold, a suitable Riemannian gradient. Given these definitions, an exact gradient step in the function space would satisfy $v_{\theta_{t+1}} = v_{\theta_t} - \eta r$ for

some step size η . Applying the first-order approximation $v_{\theta_{t+1}} \approx v_{\theta_t} + J(\theta_{t+1} - \theta_t)$ and rearranging yields the *natural gradient subproblem*

$$J\theta_{t+1} = J\theta_t - \eta r. \quad (3)$$

In practice, the model Jacobian J is not of full row rank and so the system must be solved by minimizing an appropriate function space distance metric. The most common approach is to use the L^2 distance and also incorporate Tikhonov regularization to yield the iteration

$$\begin{aligned} \theta_{t+1} &= \arg \min_{\theta} \|J\theta - (J\theta_t - \eta r)\|^2 + \lambda \|\theta - \theta_t\|^2 \quad (4) \\ &= \theta_t - \eta(J^\top J + \lambda I)^+ J^\top r, \end{aligned} \quad (5)$$

where we have used the Moore-Penrose pseudoinverse to smoothly handle the case when $\lambda = 0$ and J is not of full column rank. Here $J^\top J$ is known as the Fisher information matrix and the chain rule implies $J^\top r = \nabla_\theta \mathcal{L}(v_{\theta_t})$, so this formulation agrees with the standard preconditioner-based formulation of L^2 natural gradient descent. It also matches with the natural gradient algorithms that have been most effective for both NNWs and PINNs, which are commonly known as stochastic reconfiguration (Sorella, 2001) and energy natural gradient descent (Müller & Zeinhofer, 2023), respectively. See (Amari, 1998; Martens, 2020) for alternative discussions of the natural gradient method.

3.2. Sampling and Subsampling

To make natural gradient methods practical we can sample both the function space gradient r and the model Jacobian J by drawing k samples from the domain of \mathcal{H} and using these samples, S , to instantiate the corresponding rows $r_S \in \mathbb{R}^k$, $J_S \in \mathbb{R}^{k \times n}$. In particular we use

$$r_S = \begin{bmatrix} [\nabla_v \mathcal{L}(v_\theta)](S_1) \\ \vdots \\ [\nabla_v \mathcal{L}(v_\theta)](S_k) \end{bmatrix}, \quad J_S = \begin{bmatrix} \nabla_\theta v_\theta(S_1)^\top \\ \vdots \\ \nabla_\theta v_\theta(S_k)^\top \end{bmatrix} \quad (6)$$

where $S = \{S_1, \dots, S_k\}$. In practice the entries of r_S can be computed efficiently as long as \mathcal{L} has a local structure, while the rows of J_S can be computed efficiently by backpropagating through the model. We note that when S is sampled from a non-uniform distribution it may be appropriate to rescale the rows of J_S, r_S via importance sampling, but for clarity we focus on the case without any rescaling. We also note that in the case of NNWs, both r_S and J_S include a normalization term which must be estimated stochastically. However, for our analysis we assume exact access to r_S and J_S ,

The *subsampled* regime refers to the case when the sample size k is smaller than the number of parameters n , so that J_S is wider than it is tall. For example, a canonical application

might use $k = 10^3$ samples to optimize $n = 10^6$ parameters. In such settings, substituting J_S and r_S into the regularized least-squares problem (4) yields an efficient subsampled natural gradient (SNG) algorithm:

$$\begin{aligned}\theta_{t+1} &= \arg \min_{\theta} \|J_S \theta - (J_S \theta_t - \eta r_S)\|^2 + \lambda \|\theta - \theta_t\|^2 \\ &= \theta_t - \eta J_S^\top (J_S J_S^\top + \lambda I)^+ r_S\end{aligned}$$

In addition to the efficiency gains from the sampling itself, this formulation only requires inverting a $k \times k$ kernel matrix in sample space rather than an $n \times n$ preconditioner matrix in parameter space, resulting in a dramatic reduction in the iteration cost.

To simplify the formulas we define the compressed notation

$$J_S^{+(\lambda)} = J_S^\top (J_S J_S^\top + \lambda I)^+, \quad (7)$$

which should be viewed as a regularized version of the pseudoinverse since $J_S^{+(0)} = J_S^+$. This enables us to write the SNG iteration succinctly as

$$\theta_{t+1} = \theta_t - \eta J_S^{+(\lambda)} r_S. \quad (8)$$

We note that although the values of r, J, S change at each iteration, we keep this dependence implicit to avoid clutter.

3.3. Sketch-and-Project

Sketch-and-project methods solve a linear system $J\theta = b$ by repeatedly applying a sketching matrix Ω on the left and then projecting the current iterate onto the solution space of the sketched equation $\Omega J\theta = \Omega b$ (Gower & Richtárik, 2015). Applying this operation using standard orthogonal projections leads to the iterative method

$$\theta_{t+1} = \theta_t + (\Omega_t J)^+ (\Omega_t b - \Omega_t J \theta_t). \quad (9)$$

In this work, we are most interested in the special case known as the randomized block Kaczmarz method (Needell & Tropp, 2014), which arises by choosing $\Omega_t = I_S$ so that $\Omega_t J = J_S$ and $\Omega_t b = b_S$ represent subsets of the rows of J and b . The resulting iteration then takes the form

$$\theta_{t+1} = \theta_t + J_S^+ (b_S - J_S \theta_t). \quad (10)$$

It is also possible to incorporate regularization into the randomized block Kaczmarz iterations to yield the formula

$$\theta_{t+1} = \theta_t + J_S^{+(\lambda)} (b_S - J_S \theta_t). \quad (11)$$

Such regularization has been shown to yield improved stability for inconsistent linear systems (Goldshlager et al., 2025) and to enable optimal convergence rates in the presence of Nesterov acceleration (Dereziński et al., 2025b). We emphasize that the regularization here is internal to the iterations

and does *not* imply that the algorithm targets a regularized solution to the original linear system.

The standard convergence result for sketch-and-project methods, Theorem 4.6 of (Gower & Richtárik, 2015), states that when there is a unique θ^* satisfying $J\theta^* = b$, it holds

$$\mathbb{E} \|\theta_t - \theta^*\|^2 \leq (1 - \alpha)^t \|\theta_0 - \theta^*\|^2 \quad (12)$$

with

$$\alpha = \lambda_{\min}^+(\bar{P}), \quad \bar{P} = \mathbb{E}_S [P(S)], \quad P(S) = J_S^{+(\lambda)} J_S. \quad (13)$$

In words, $P(S)$ is a regularized projector onto the row space of J_S , \bar{P} is the expectation of this projector, and α is the minimal eigenvalue of the expected projector. We highlight that the expected projector \bar{P} and the convergence rate α will play a significant role in our analysis of SNG.

A major strength of sketch-and-project methods is that the rate constant α can be insensitive to the largest k singular values of J , and it can thus scale *superlinearly* in the sample size in the presence of fast spectral decay. See for example (Dereziński & Rebrova, 2024) (Lemma 3.3 and Corollary 3.4), (Dereziński et al., 2025a;b), and (Goldshlager et al., 2025) (Theorem E.1 and related discussions).

3.4. Squared Volume Sampling

Given a matrix J , a sample size k , and a regularization parameter $\lambda \geq 0$, squared volume sampling (SVS) selects k rows from J with indices S with a probability proportional to the squared volume of the parallelepiped formed by the rows of $[J_S \sqrt{\lambda} I]$. Concretely we define the distribution $\text{SVS}(J, k, \lambda)$ to have probability mass function

$$p(S) = \frac{\det(J_S J_S^\top + \lambda I)}{\sum_{|S'|=k} \det(J_{S'} J_{S'}^\top + \lambda I)} \quad (14)$$

when $|S| = k$, and 0 otherwise. We note that when $\lambda = 0$ it is required that $k \leq \text{rank}(J)$, and we also remark that SVS is a special case of a determinantal point process (DPP).

Various algorithms have been proposed to implement squared volume sampling, including both direct and Markov chain Monte Carlo approaches; see (Dereziński & Mahoney, 2021) for an overview. However, our main interest in SVS not as a practical sampling strategy, but rather as a tool to enable theoretical insight into algorithms which are otherwise difficult to analyze. SVS has previously been used in this way for both randomized block coordinate descent methods (Mutny et al., 2020; Rodomanov & Kropotov, 2020) and randomized block Kaczmarz methods (Dereziński et al., 2025b; Goldshlager et al., 2025; Xiang et al., 2025). In both cases, the power of SVS is that it enables exact computations of expectation values involving the inverse of a subsampled matrix, which are otherwise challenging to control. We will use this same property to provide new insights into subsampled natural gradient algorithms.

3.5. Related Works

Several works have made connections between subsampled Newton algorithms and sketch-and-project methods (Qu et al., 2016; Rathore et al., 2024), with one even considering a variant of squared volume sampling (Mutny et al., 2020). Another work has analyzed a subsampled Gauss-Newton algorithm for overparameterized neural networks in a non-linear least-squares setting (Cai et al., 2019). In the context of natural gradient methods, one recent work considered the use of squared volume sampling (Gruhlke et al., 2024), but this work focused on the oversampled regime in which there are more samples than parameters, which is qualitatively different than the subsampled regime.

4. Analysis without Decoupling

We now begin our work by considering the primary barrier to providing theoretical insight using the sketch-and-project approach: namely, how to rigorously guarantee the convergence without decoupling the gradient from the preconditioner. To start, we note that the SNG iteration (8) can be derived by applying a regularized block Kaczmarz step (11) to the natural gradient subproblem (3):

$$\begin{aligned}\theta_{t+1} &= \theta_t + J_S^{+(\lambda)}((J\theta_t - \eta r)_S - J_S\theta_t) \\ &= \theta_t - \eta J_S^{+(\lambda)}r_S.\end{aligned}$$

This forms the basis for the sketch-and-project interpretation of SNG, and it implies rigorous convergence guarantees such as (12) for consistent linear least-squares problems. However, it is not trivial to extend such guarantees to more general settings when both the left- and right-hand side of the linear system are changing at each iteration.

To clarify the problem we write the expected direction as

$$\mathbb{E} \left[J_S^{+(\lambda)}r_S \right] = J^\top \bar{W}r \quad (15)$$

where $\bar{W} = \mathbb{E}_S [I_S^\top (J_S J_S^\top + \lambda I)^+ I_S] \succeq 0$. To guarantee the convergence using standard techniques, we would like to pass \bar{W} to the left as $J^\top \bar{W}r = \tilde{W}J^\top r$ to obtain a preconditioned gradient descent direction. Unfortunately it is difficult to guarantee that this manipulation is possible under general conditions.

In fact, it is exactly this challenge that has lead previous analyses to study a theoretical proxy of the form

$$\theta_{t+1} = \theta_t - \eta (J_{S'}^\top J_S + \lambda I)^+ J_S^\top r_S \quad (16)$$

where S, S' are two independent mini-batches. This form is justified as a plug-in estimator for the deterministic algorithm (5), and when $S = S'$ it becomes equivalent to the practical single mini-batch algorithm due to the push-through identity $(J_S^\top J_S + \lambda I)^+ J_S^\top = J_S^\top (J_S J_S^\top + \lambda I)^+$.

The problem with this proxy is that the resulting analyses fail to provide insight into realistic small-sample settings. The reason is that the stochastic preconditioner $J_{S'}^\top J_S$ has a rank of at most $k \ll n$ and is thus unlikely to be informative for the independently estimated stochastic gradient $J_S^\top r_S$. In other words, the coupling which is broken by introducing S' is in fact essential to the functioning of the algorithm.

Motivated by the failure of the two mini-batch proxy, we return to the single mini-batch algorithm and search for another way to facilitate the analysis. In particular, the interpretation of SNG as a randomized block Kaczmarz method suggests the consideration of a new proxy based on squared volume sampling (SVS). This proxy is promising since SVS is known to enable exact computations of expectation values along the lines of (15), and we find that it is indeed sufficient to address the challenge at hand:

Lemma 4.1. *Let $J \in \mathbb{R}^{m \times n}$, $r \in \mathbb{R}^m$, and $S \sim \text{SVS}(J, k, \lambda)$. Then it holds*

$$\mathbb{E}_S \left[J_S^{+(\lambda)}r_S \right] = \tilde{W}J^\top r, \quad (17)$$

with $\tilde{W} = (J^\top J)^{-1/2} \bar{P} (J^\top J)^{-1/2}$ and \bar{P} as in (13).

In other words, under SVS the expectation of the SNG direction $J_S^{+(\lambda)}r_S$ becomes equal to a preconditioned gradient descent step, *without* decoupling the gradient and the preconditioner. Moreover, the SNG preconditioner arises by combining the expected projector \bar{P} with the natural gradient preconditioner $J^\top J$, which already suggests that the sketch-and-project structure controls the gap between SNG and its deterministic counterpart. The proof of Lemma 4.1, which follows from known expectation formulas for SVS, can be found in Appendix A. Note that here and elsewhere we use $(J^\top J)^{-1/2}$ as a shorthand for $[(J^\top J)^+]^{1/2}$.

As a first consequence of Lemma 4.1, we can now provide global convergence guarantees for SNG without invoking two independent mini-batches. The assumptions to ensure global convergence can be formulated in a variety of ways; to provide just one example we present the following result:

Theorem 4.2 (Global convergence of SVS-SNG). *Consider an instance of the parametric optimization problem (1) such that $\mathcal{H} = \mathbb{R}^m$. Suppose that $\mathcal{L}(v_\theta)$ is bounded below and is continuously differentiable as a function of θ , and also that $v_\theta, \nabla_\theta \mathcal{L}(v_\theta)$ are Lipschitz continuous as a function of θ . Suppose additionally that there exist constants $C_1, C_2 > 0$ such that $\|r\|^2 \leq C_1 \|J^\top r\|^2 + C_2$ for all θ .*

Then under the sampling distribution $S \sim \text{SVS}(J, k, \lambda)$, a positive regularization $\lambda > 0$, and diminishing step sizes η_t satisfying $\sum_{t=1}^\infty \eta_t = \infty$ and $\sum_{t=1}^\infty \eta_t^2 < \infty$, it holds

$$\lim_{T \rightarrow \infty} \mathbb{E} \left[\frac{1}{\sum_{t=1}^T \eta_t} \sum_{t=1}^T \eta_t \|\nabla_\theta \mathcal{L}(v_{\theta_t})\|^2 \right] = 0.$$

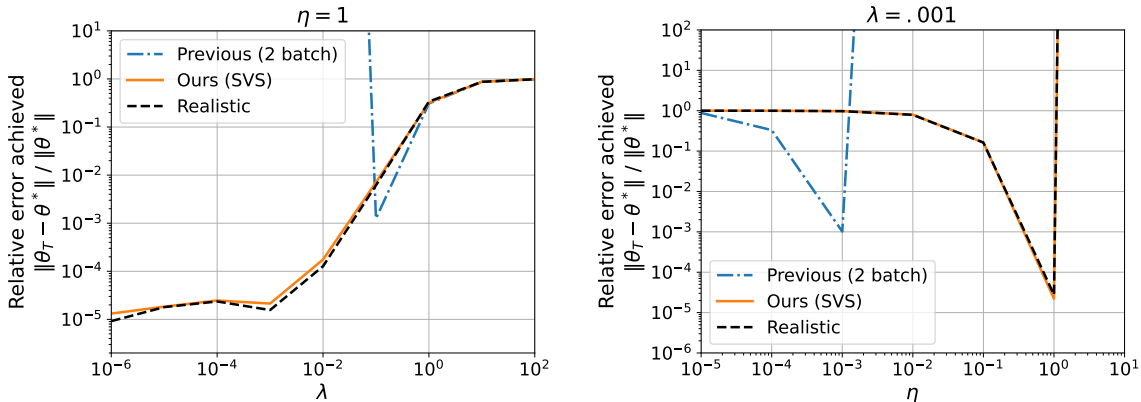


Figure 2. Empirical performance of two theoretical proxies for SNG relative to a realistic algorithm using a single, uniformly sampled mini-batch. The results are for a consistent instance of linear least-quadratics involving random Gaussian matrices and the behavior is tested for a fixed step size η and varying regularizations λ (left), as well as for fixed λ and varying η (right). In both cases the behavior of SVS-SNG matches closely with the realistic algorithm, while the behavior of the two mini-batch proxy is entirely distinct. The dimensions are $m = 10^3$, $n = 10^2$, and $k = 10$, which is small enough to directly implement SVS. The y -axis represents the relative error achieved after $T = 10^3$ iterations. See also Appendix E for an ablation regarding non-Gaussian data.

The only unusual part of this result is the condition on $\|r\|^2$, which is used to ensure that the variance of the sketch-and-project step can be controlled in terms of the size of the gradient $J^\top r$. To see that this condition is reasonable, we note every LLQ instance admits values of C_1 and C_2 such that the condition holds, as proved in Proposition B.2. The proof of Theorem 4.2 is also presented in Appendix B and follows by showing that under SVS, SNG satisfies the assumptions of Theorem 4.1 of (Bottou et al., 2018). We emphasize that SVS is merely a *sufficient* condition for these assumptions, and it is possible that other sampling distributions can also satisfy these assumptions under appropriate conditions.

The main value of Lemma 4.1 and Theorem 4.2 is in establishing SVS-SNG as a *new theoretical proxy* for understanding SNG. The suitability of SVS as a proxy is supported by previous analyses of randomized block Kaczmarz methods which show that under benign conditions, SVS can behave similarly to uniform sampling (Dereziński et al., 2025b; Goldshlager et al., 2025). We further provide numerical evidence that this similarity can extend to the case of SNG, with results for Gaussian data in Figure 2 and an ablation regarding non-Gaussian data in Appendix E.

Regarding the practical implications, we do not suggest that SVS should be implemented directly, since even the most efficient algorithms for doing so still require accessing either all of J or a large number of rows of J in order to generate each mini-batch. However, the idea of SVS may still motivate new practical directions, for example by suggesting the incorporation of negative correlations between the samples within each mini-batch. Such an approach is not far-fetched, particularly for applications such as NNWs in which the samples are already generated from a Markov chain Monte

Carlo process. We view such directions as quite promising, but we defer their exploration to future works since our focus is on theoretical insight.

5. Small-Sample Insights

We now turn our attention to our main goal of providing detailed insights into small-sample settings. For this purpose we focus on the linear least-quadratics setting (LLQ), which we recall is motivated by the search for high-precision solutions and is derived as a second-order approximation to general consistent parametric optimization problems. For clarity and since the motivation for the model problem comes from the consistent regime, we focus on consistent instances of LLQ. However, our results can be easily extended to inconsistent instances following the ideas of (Epperly et al., 2025; Goldshlager et al., 2025). Our results can also be extended to yield local convergence rates for consistent instances of the general problem (1) as long as both J and H are Lipschitz continuous functions of θ ; see (Roosta-Khorasani & Mahoney, 2019; Martens, 2020) for relevant arguments. We also note that throughout this section we uniquely define $\theta^* = \min_{\theta \in \text{range}(J^\top)} \mathcal{L}(v_\theta)$.

Within the consistent LLQ setting, the key challenge lies in handling the interaction between (i) the sketch-and-project structure induced by the Jacobian J , and (ii) the natural gradient structure induced by the Hessian H . Fortunately, we already know from Lemma 4.1 that under SVS, the expectation of each SNG iteration takes the form of a preconditioned gradient descent step. This enables us to extend existing sketch-and-project analyses to ensure a steady reduction in the solution error when measured in an appropriate norm:

Theorem 5.1 (Convergence of SVS-SNG for LLQ). *Consider a consistent instance of linear least-quadratics and assume an initial guess of $\theta_0 \in \text{range}(J^\top)$. Define \bar{P} , α as in (13), \tilde{W} as in Lemma 4.1, and a new quantity*

$$\gamma = \left\| \mathbb{E}_S \left[I_S^\top (J_S^{+(\lambda)})^\top \tilde{W}^+ J_S^{+(\lambda)} I_S \right] \right\|_2 \quad (18)$$

which relates to the second moment of the sketch-and-project step.

Then when $S \sim \text{SVS}(J, k, \lambda)$ and $\eta \leq 1/(\gamma \|H\|_2)$, it holds

$$\mathbb{E} \|\theta_t - \theta^*\|_{\tilde{W}^+}^2 \leq (1 - \eta \cdot \lambda_{\min}(H) \cdot \alpha)^t \|\theta_0 - \theta^*\|_{\tilde{W}^+}^2. \quad (19)$$

The proof of Theorem 5.1 can be found in Appendix C. Importantly, although \tilde{W}^+ is not necessarily full rank, it does act as a norm on the subspace $\text{range}(J^\top)$, which contains all the error vectors as established by Lemma C.1. As a result, Theorem 5.1 provides a genuine linear convergence rate for SVS-SNG for LLQ. We note that unlike Theorem 4.2, which ultimately relies on inequality conditions that might be met by more general sampling distributions, Theorem 5.1 directly leverages the exact expectation formula of Lemma 4.1 and can thus be more difficult to generalize.

To understand the meaning of Theorem 5.1 it is helpful to compare with deterministic natural gradient descent:

Corollary 5.2 (Convergence of NGD for LLQ). *Consider a consistent instance of linear least-quadratics and assume an initial guess of $\theta_0 \in \text{range}(J^\top)$. Then when $\lambda = 0$ and $\eta \leq 1/\|H\|_2$, deterministic natural gradient descent satisfies*

$$\mathbb{E} \|\theta_t - \theta^*\|_{J^\top J}^2 \leq (1 - \eta \cdot \lambda_{\min}(H))^t \|\theta_0 - \theta^*\|_{J^\top J}^2. \quad (20)$$

The proof of Corollary 5.2, which is a direct specialization of Theorem 5.1, can be found in Appendix C.

Overall, these results provide the first characterization of the convergence properties of SNG in small-sample settings. In particular, comparing Corollary 5.2 to Theorem 5.1 reveals that under SVS, the effect of subsampling is to (i) reduce the maximum stable step size by a factor of γ , and (ii) reduce the convergence rate by an additional factor of α . This means that as the sample size is varied, the optimal rate scales as α/γ . Furthermore, while our proofs rely on SVS, we emphasize that the suggested mechanisms are interpretable under much more general conditions, since α and γ can be defined according to any chosen sampling distribution.

Importantly, the appearance of α in Theorem 5.1 enables us to draw insights from the rich body of literature on sketch-and-project methods. For example, based on this literature we can immediately suggest a new explanation for the success of SNG in scientific machine learning, since (i) it is

known that α can scale superlinearly in the sample size when J exhibits fast spectral decay (see Section 3.3), and (ii) J is commonly observed to exhibit fast spectral decay in practice (Park & Kastoryano, 2020; Wang et al., 2022). This provides a distinct advantage relative to SGD, which enjoys at best linear scaling (Jain et al., 2018). Furthermore, since the scaling of α is limited only by the spectral decay rate, this superlinear scaling can easily compensate for SNG’s increased iteration cost of $\mathcal{O}(k^2)$ rather than $\mathcal{O}(k)$. It is also worth noting that the superlinear scaling of α can occur independently of any changes to the step size η , which depends only on H and γ . This again contrasts with SGD, for which the step size must always be increased to reap the benefits of larger mini-batches (Jain et al., 2018).

The other sketch-and-project quantity, γ , has not appeared in previous analyses. Intuitively, the effect of γ is to modulate the benefits of the sketch-and-project structure, since when $\gamma = \mathcal{O}(1)$ the sketch-and-project rate α can cleanly extend into the natural gradient setting, whereas when $\gamma \gg 1$ the rate suffers from the transition. Structurally, γ is related to the second moment of the sketch-and-project step and is similar to second-moment quantities which have appeared in analyses of accelerated sketch-and-project methods (Gower et al., 2018; Dereziński et al., 2025b). As discussed in Section 6, such second-moment quantities can admit favorable upper bounds in benign cases, which suggests that γ may also behave benignly under appropriate conditions.

Unfortunately, proving such a result can be quite technical and is outside the scope of the current work. For now we present the following preliminary characterizations:

Proposition 5.3. *Define γ as in Theorem 5.1. Then:*

1. *If $\lambda=0$, $S \sim \text{SVS}(J, k, \lambda)$, and $k=1$ or $k=m$, then $\gamma=1$.*
2. *If $\lambda>0$ and S is uniform, then $\gamma \leq 1 + \frac{1}{\lambda} \max_i \|J_i\|^2$.*

The proof of Proposition 5.3 is presented in Appendix C. These results put some limits on the extent to which γ can suppress the superlinear scaling enjoyed by α , but they are not tight enough to fully clarify the behavior. To supplement these preliminary bounds, we provide an additional proposition showing that the influence of γ can disappear under a strong compatibility condition:

Proposition 5.4 (Convergence under strong compatibility). *Consider a consistent instance of linear least-quadratics and assume an initial guess $\theta_0 \in \text{range}(J^\top)$. Set the sampling distribution to be $\text{SVS}(J, k, \lambda)$ and assume a strong compatibility condition $[H, J J^\top] = 0$. Then with step size $\eta \leq 1/\|H\|_2$ the SNG iterates satisfy*

$$\mathbb{E} \|\theta_t - \theta^*\|^2 \leq (1 - \eta \cdot \lambda_{\min}(H) \cdot \alpha)^t \|\theta_0 - \theta^*\|^2, \quad (21)$$

with α as in (13).

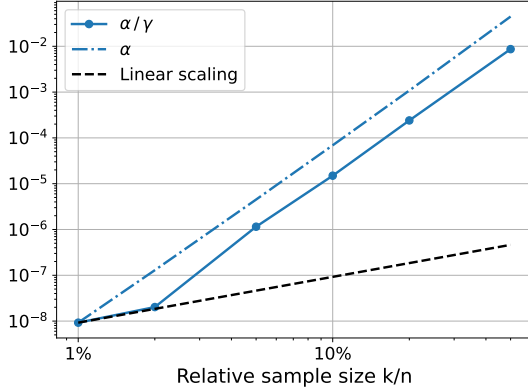


Figure 3. Empirical scaling of the convergence parameters α and γ as a function of the sample size k , under SVS. The results are for a random Gaussian Jacobian matrix with quadratic spectral decay. The sketch-and-project constant α grows superlinearly as predicted, and the presence of γ only mildly impedes this superlinear scaling. The regularization is set to $\lambda = 0$ for simplicity and the dimensions are $m = 10^3$ and $n = 10^2$, which is small enough to (i) calculate α directly using symmetric polynomials, and (ii) estimate γ by sampling directly from $\text{SVS}(J, k, \lambda)$.

The proof of Proposition 5.4 can be found in Appendix C. The result is that in at least one special case, the advantages of sketch-and-project methods can extend to a genuine natural gradient setting without qualification.

To wrap up our discussion of γ , we provide a numerical experiment which explores the behavior of α and γ under SVS, for a random Gaussian J matrix with quadratic spectral decay. The results in Figure 3 show that γ exerts only a mild damping effect on the predicted convergence rate, with α/γ still growing superlinearly.

Finally, we directly investigate the suggestion that SNG can exploit spectral decay in the model Jacobian. To this end we test the behavior of SNG under uniform sampling for two instances of LLQ involving random Gaussian matrices. The results in Figure 4 confirm that SNG exhibits superlinear scaling exactly when J has fast spectral decay.

6. Principled Acceleration

As an additional demonstration of the power of the sketch-and-project approach, we now turn our attention to the question of acceleration. In particular, we consider the subsampled projected-increment natural gradient (SPRING) algorithm, which has recently been proposed as a structured momentum scheme for SNG (Goldshlager et al., 2024). Despite numerous applications of SPRING (Smith et al., 2024; Scherbela et al., 2025; Chen et al., 2025; Hendry et al., 2025) and several proposals to further improve the algorithm (Gu et al., 2025; Li et al., 2025), the structure and convergence properties of SPRING have remained mysterious. We clar-

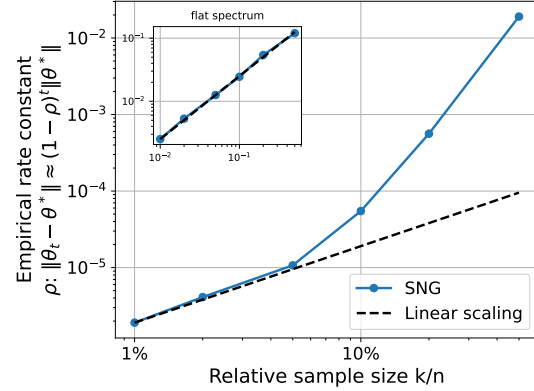


Figure 4. Empirical validation that SNG can exploit spectral decay in the model Jacobian, under uniform sampling. The results are for a consistent instance of linear least-quadratics involving random Gaussian matrices, with J exhibiting quadratic spectral decay. The empirical rate constant grows superlinearly as predicted even while the step size is fixed at $\eta = 1$. The regularization is set to $\lambda = 0$ for simplicity and the dimensions are $m = 10^3$ and $n = 10^2$. Inset: when J has a flat spectrum, the rate scales linearly.

ify the situation through the following result:

Theorem 6.1 (SPRING as accelerated sketch-and-project). *The accelerated regularized sketch-and-project algorithm for the system $J\theta = b$, as presented for example by (Gower et al., 2018; Dereziński et al., 2025b), can be reformulated as*

$$\begin{aligned}\phi_{t+1} &= \mu\phi_t + (\Omega_t J)^{+(\lambda)}(\Omega_t b - \Omega_t J(\theta_t + \mu\phi_t)), \\ \theta_{t+1} &= \theta_t + \eta\phi_{t+1}\end{aligned}\quad (22)$$

after an appropriate transformation of variables. Applying (22) to the natural gradient subproblem (3), with the standard row sampling sketching matrix I_S , yields the iteration

$$\begin{aligned}\phi_{t+1} &= \mu\phi_t + J_S^{+(\lambda)}(r_S - \mu J_S \phi_t), \\ \theta_{t+1} &= \theta_t - \eta\phi_{t+1}.\end{aligned}\quad (23)$$

This is exactly the iteration used by SPRING.

In other words, while the SPRING algorithm appears mysterious from a stochastic preconditioning perspective, it is a natural construction from the viewpoint of sketch-and-project methods. The proof of Theorem 6.1, which is straightforward once the appropriate transformation of variables is identified, can be found in Appendix D.

As a result of Theorem 6.1, Theorem 3 of (Gower et al., 2018) (or also eq. (1) of (Dereziński et al., 2025a)) implies that for a consistent linear least-squares problem SPRING satisfies a convergence bound of the form

$$\mathbb{E} \|\theta_t - \theta^*\|^2 = \mathcal{O}\left((1 - \sqrt{\alpha/\beta})^t\right) \|\theta_0 - \theta^*\|^2 \quad (24)$$

with α as in (13), \mathcal{O} indicating constant factors that do not depend on t , and β a second moment quantity defined by

$$\beta = \left\| \bar{P}^{-1/2} \mathbb{E}_S \left[J_S^\top (J_S^{+(\lambda)})^\top \bar{P}^+ J_S^{+(\lambda)} J_S \right] \bar{P}^{-1/2} \right\|_2. \quad (25)$$

The implications of this bound have been developed by several previous works (Gower et al., 2018; Dereziński et al., 2025a;b), with the overall message being that the rate constant $\sqrt{\alpha/\beta}$ can be similar to α for adversarial problems, but can scale more like $\sqrt{\alpha}$ for benign problems. Conceptually, this means that we can expect the benefits of SPRING to be greatest when α is small, or equivalently when the underlying sketch-and-project steps converge slowly. This explains the recent observation of (Guzmán-Cordero et al., 2025) that SPRING is most beneficial when the sample size is small relative to the dimensionality of the problem. Finally, we note that the benign case follows exactly from providing favorable upper bounds on β , which suggests that similar techniques could also be used to bound our γ .

We are not yet able to extend these results to the LLQ setting due to the complex interaction between Nesterov acceleration and the function space Hessian. Still, based on Theorems 5.1 and 6.1 and eqs. (12) and (24), we conjecture that SPRING always accelerates SNG by replacing α with the accelerated sketch-and-project constant $\sqrt{\alpha/\beta}$:

Conjecture 6.2 (Convergence of SVS-SPRING for LLQ). *Consider a consistent instance of linear least-quadratics and assume an initial guess of $\theta_0 \in \text{range}(J^\top)$. Then under the sampling distribution SVS(J, k, λ) and with appropriate choices of η and μ , SPRING satisfies*

$$\mathbb{E} \|\theta_t - \theta^*\|^2 = \mathcal{O} \left((1 - \kappa^{-1}(H) \cdot \sqrt{\alpha/\beta} / \gamma)^t \right) \|\theta_0 - \theta^*\|^2 \quad (26)$$

with α as in (13), β as in (25), γ as in Theorem 5.1, and \mathcal{O} indicating constant factors that do not depend on t .

We defer the resolution of this conjecture to future works. For now, we provide numerical experiments exploring the convergence of SPRING in the LLQ setting, with results in Figure 5. We find that SPRING provides substantial acceleration for small sample sizes, but the gap shrinks as the sample size is increased. This is consistent with Conjecture 6.2 since large sample sizes correspond exactly to larger values of α , which should thus reduce the opportunity for acceleration.

Interestingly, we do *not* predict or observe SPRING to achieve an improvement in the dependence on the condition number $\kappa(H)$. Identifying algorithms that do, perhaps achieving convergence rates scaling with $\kappa^{-1/2}(H)$, for example by introducing acceleration in the function space (Li et al., 2025), is a promising direction for future works.

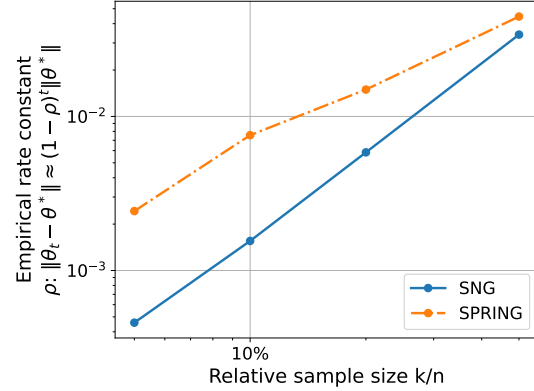


Figure 5. Empirical comparison of the convergence rates of SNG and SPRING for a variety of sample sizes. The results are for a consistent instance of linear least-quadratics in which J and H both have linearly decaying spectra. As suggested by Conjecture 6.2, SPRING provides substantial acceleration for small sample sizes, but the gap shrinks as the sample size is increased. The regularization is set to $\lambda = 0$ for simplicity and the dimensions are $m = 10^3$, $n = 10^2$. Furthermore, the hyperparameters η and μ are tuned independently for each run.

Conclusions

In this work we have demonstrated that subsampled natural gradient algorithms can be more fruitfully understood as sketch-and-project methods rather than stochastic preconditioning schemes. Building on this perspective we have shown how to analyze SNG without decoupling the gradient and the preconditioner, provided the first meaningful characterization of how subsampling affects the convergence rate of natural gradient descent, and clarified the mechanism behind the SPRING algorithm. Overall, our findings suggest that when using subsampled natural gradient algorithms to solve scientific machine learning problems, more attention should be paid to the sketch-and-project properties such as α and γ , and less to the statistical estimation properties such as the variance of the gradient and preconditioner estimates.

Looking forward, our work sets the stage for a broader effort to leverage ideas from randomized linear algebra to develop and analyze subsampled optimizers for scientific machine learning. Theoretically, promising directions include providing tighter bounds on γ , verifying Conjecture 6.2, proposing acceleration schemes that attain convergence rates scaling with $\kappa^{-1/2}(H)$, and exploring how to relax our SVS assumption. Practically, future works should explore sampling algorithms inspired by SVS, for example by using ensemble samplers (Goodman & Weare, 2010) to introduce negative correlation within each mini-batch. They should also consider incorporating other tools from the sketch-and-project literature such as adaptive acceleration (Dereziński et al., 2025b), tail averaging (Epperly et al., 2025), and oblique projections (Gower & Richtárik, 2015).

Acknowledgements

This material is based upon work supported by the U.S. Department of Energy, Office of Science, Office of Advanced Scientific Computing Research, Department of Energy Computational Science Graduate Fellowship under Award Number DE-SC0023112 (G.G.). This work was supported by a grant from the Simons Foundation [SFI-MPS-SDF-00014421, G.G.] and by a Hearts to Humanity Eternal graduate research grant (G.G.). This work was supported in part by the U.S. Department of Energy, Office of Science, Office of Advanced Scientific Computing Research’s Applied Mathematics Competitive Portfolios program under Contract No. AC02-05CH11231 (L.L.), and by the Simons Investigator in Mathematics award through Grant No. 825053 (J.H., L.L.). We thank Ethan Epperly, James Larsen, Michal Dereziński, and Marius Zeinhofer for helpful discussions.

References

- Amari, S.-I. Natural gradient works efficiently in learning. *Neural computation*, 10(2):251–276, 1998.
- Bollapragada, R., Byrd, R. H., and Nocedal, J. Exact and inexact subsampled Newton methods for optimization. *IMA Journal of Numerical Analysis*, 39(2):545–578, 2019.
- Bottou, L., Curtis, F. E., and Nocedal, J. Optimization methods for large-scale machine learning. *SIAM review*, 60(2):223–311, 2018.
- Cai, T., Gao, R., Hou, J., Chen, S., Wang, D., He, D., Zhang, Z., and Wang, L. Gram-Gauss-Newton method: Learning overparameterized neural networks for regression problems. *arXiv preprint arXiv:1905.11675*, 2019.
- Carleo, G. and Troyer, M. Solving the quantum many-body problem with artificial neural networks. *Science*, 355(6325):602–606, 2017.
- Chen, A. and Heyl, M. Empowering deep neural quantum states through efficient optimization. *Nature Physics*, 20(9):1476–1481, 2024.
- Chen, A., Wan, Z.-Q., Sengupta, A., Georges, A., and Roth, C. Neural network-augmented Pfaffian wave-functions for scalable simulations of interacting fermions. *arXiv preprint arXiv:2507.10705*, 2025.
- Dangel, F., Müller, J., and Zeinhofer, M. Kronecker-factored approximate curvature for physics-informed neural networks. *Advances in Neural Information Processing Systems*, 37:34582–34636, 2024.
- Dereziński, M. and Mahoney, M. W. Determinantal point processes in randomized numerical linear algebra. *Notes of the American Mathematical Society*, 68(1):34–45, 2021.
- Dereziński, M. and Rebrova, E. Sharp analysis of sketch-and-project methods via a connection to randomized singular value decomposition. *SIAM Journal on Mathematics of Data Science*, 6(1):127–153, 2024.
- Dereziński, M. and Yang, J. Solving dense linear systems faster than via preconditioning. In *Proceedings of the 56th Annual ACM Symposium on Theory of Computing*, pp. 1118–1129, 2024.
- Dereziński, M., LeJeune, D., Needell, D., and Rebrova, E. Fine-grained analysis and faster algorithms for iteratively solving linear systems. *Journal of Machine Learning Research*, 26(144):1–49, 2025a.
- Dereziński, M., Needell, D., Rebrova, E., and Yang, J. Randomized Kaczmarz methods with beyond-Krylov convergence. *SIAM Journal on Matrix Analysis and Applications*, 46(4):2558–2588, 2025b.
- Epperly, E. N., Goldshlager, G., and Webber, R. J. Randomized Kaczmarz with tail averaging. *Applied and Computational Harmonic Analysis*, pp. 101812, 2025.
- Foulkes, W. M., Mitas, L., Needs, R., and Rajagopal, G. Quantum Monte Carlo simulations of solids. *Reviews of Modern Physics*, 73(1):33, 2001.
- Goldshlager, G., Abrahamsen, N., and Lin, L. A Kaczmarz-inspired approach to accelerate the optimization of neural network wavefunctions. *Journal of Computational Physics*, 516:113351, 2024.
- Goldshlager, G., Hu, J., and Lin, L. Worth their weight: Randomized and regularized block Kaczmarz algorithms without preprocessing. *arXiv preprint arXiv:2502.00882*, 2025.
- Goodman, J. and Weare, J. Ensemble samplers with affine invariance. *Communications in applied mathematics and computational science*, 5(1):65–80, 2010.
- Gower, R., Hanzely, F., Richtárik, P., and Stich, S. U. Accelerated stochastic matrix inversion: general theory and speeding up BFGS rules for faster second-order optimization. *Advances in Neural Information Processing Systems*, 31, 2018.
- Gower, R. M. and Richtárik, P. Randomized iterative methods for linear systems. *SIAM Journal on Matrix Analysis and Applications*, 36(4):1660–1690, 2015.
- Gruhlke, R., Nouy, A., and Trunschke, P. Optimal sampling for stochastic and natural gradient descent. *arXiv preprint arXiv:2402.03113*, 2024.

- Gu, Y., Li, W., Lin, H., Zhan, B., Li, R., Huang, Y., He, D., Wu, Y., Xiang, T., Qin, M., et al. Solving the Hubbard model with neural quantum states. *arXiv preprint arXiv:2507.02644*, 2025.
- Guzmán-Cordero, A., Dangel, F., Goldshlager, G., and Zeinhofer, M. Improving energy natural gradient descent through Woodbury, momentum, and randomization. *arXiv preprint arXiv:2505.12149*, 2025.
- Hendry, D., Sinibaldi, A., and Carleo, G. Grassmann variational Monte Carlo with neural wave functions. *arXiv preprint arXiv:2507.10287*, 2025.
- Jain, P., Kakade, S. M., Kidambi, R., Netrapalli, P., and Sidford, A. Parallelizing stochastic gradient descent for least squares regression: mini-batching, averaging, and model misspecification. *Journal of machine learning research*, 18(223):1–42, 2018.
- Jnini, A. and Vella, F. Dual natural gradient descent for scalable training of physics-informed neural networks. *arXiv preprint arXiv:2505.21404*, 2025.
- Lange, H., Böhler, A., Roth, C., and Bohrdt, A. Simulating the two-dimensional t-J model at finite doping with neural quantum states. *Physical Review Letters*, 135(13):136504, 2025.
- Li, C., Zhu, S., Xie, Z., and Wen, Z. Accelerated natural gradient method for parametric manifold optimization. *arXiv preprint arXiv:2504.05753*, 2025.
- Lin, J., Goldshlager, G., and Lin, L. Explicitly antisymmetrized neural network layers for variational Monte Carlo simulation. *Journal of Computational Physics*, 474:111765, 2023.
- Martens, J. New insights and perspectives on the natural gradient method. *Journal of Machine Learning Research*, 21(146):1–76, 2020.
- Misery, A., Gravina, L., Santini, A., and Vicentini, F. Looking elsewhere: improving variational Monte Carlo gradients by importance sampling. *Machine Learning: Science and Technology*, 2025.
- Müller, J. and Zeinhofer, M. Achieving high accuracy with PINNs via energy natural gradient descent. In *International Conference on Machine Learning*, pp. 25471–25485. PMLR, 2023.
- Müller, J. and Zeinhofer, M. Position: Optimization in SciML should employ the function space geometry. In *International Conference on Machine Learning*, pp. 36705–36722. PMLR, 2024.
- Mutny, M., Dereziński, M., and Krause, A. Convergence analysis of block coordinate algorithms with determinantal sampling. In *International Conference on Artificial Intelligence and Statistics*, pp. 3110–3120. PMLR, 2020.
- Needell, D. and Tropp, J. A. Paved with good intentions: analysis of a randomized block Kaczmarz method. *Linear Algebra and its Applications*, 441:199–221, 2014.
- Park, C.-Y. and Kastoryano, M. J. Geometry of learning neural quantum states. *Physical Review Research*, 2(2):023232, 2020.
- Pfau, D., Spencer, J. S., Matthews, A. G., and Foulkes, W. M. C. Ab initio solution of the many-electron Schrödinger equation with deep neural networks. *Physical review research*, 2(3):033429, 2020.
- Qu, Z., Richtárik, P., Takác, M., and Fercoq, O. SDNA: Stochastic dual Newton ascent for empirical risk minimization. In *International Conference on Machine Learning*, pp. 1823–1832. PMLR, 2016.
- Raissi, M., Perdikaris, P., and Karniadakis, G. E. Physics-informed neural networks: A deep learning framework for solving forward and inverse problems involving nonlinear partial differential equations. *Journal of Computational physics*, 378:686–707, 2019.
- Rathore, P., Frangella, Z., Yang, J., Dereziński, M., and Udell, M. Have ASkotch: A neat solution for large-scale kernel ridge regression. *arXiv preprint arXiv:2407.10070*, 2024.
- Ren, Y. and Goldfarb, D. Efficient subsampled Gauss-Newton and natural gradient methods for training neural networks. *arXiv preprint arXiv:1906.02353*, 2019.
- Rende, R., Viteritti, L. L., Bardone, L., Becca, F., and Goldt, S. A simple linear algebra identity to optimize large-scale neural network quantum states. *Communications Physics*, 7(1):260, 2024.
- Rodomanov, A. and Kropotov, D. A randomized coordinate descent method with volume sampling. *SIAM Journal on Optimization*, 30(3):1878–1904, 2020.
- Roosta-Khorasani, F. and Mahoney, M. W. Sub-sampled Newton methods. *Mathematical Programming*, 174(1):293–326, 2019.
- Schätzle, Z., Szabó, P. B., Mezera, M., Hermann, J., and Noé, F. DeepQMC: An open-source software suite for variational optimization of deep-learning molecular wave functions. *The Journal of Chemical Physics*, 159(9), 2023.

- Scherbela, M., Gao, N., Grohs, P., and Günnemann, S. Accurate ab-initio neural-network solutions to large-scale electronic structure problems. *arXiv preprint arXiv:2504.06087*, 2025.
- Schwencke, N. and Furtlehner, C. ANaGRAM: A natural gradient relative to adapted model for efficient PINNs learning. In *The Thirteenth International Conference on Learning Representations*.
- Sinibaldi, A., Mello, A. F., Collura, M., and Carleo, G. Non-stabilizerness of neural quantum states. *arXiv preprint arXiv:2502.09725*, 2025.
- Smith, C., Chen, Y., Levy, R., Yang, Y., Morales, M. A., and Zhang, S. Unified variational approach description of ground-state phases of the two-dimensional electron gas. *Physical Review Letters*, 133(26):266504, 2024.
- Sorella, S. Generalized Lanczos algorithm for variational quantum Monte Carlo. *Physical Review B*, 64(2):024512, 2001.
- Vecsei, P. M. and Lado, J. L. Phase diagram of the J1-J2 Heisenberg second-order topological quantum magnet. *Physical Review Research*, 7(1):013194, 2025.
- Wang, S., Yu, X., and Perdikaris, P. When and why PINNs fail to train: A neural tangent kernel perspective. *Journal of Computational Physics*, 449:110768, 2022.
- Wu, J., Hu, J., Zhang, H., and Wen, Z. Convergence analysis of an adaptively regularized natural gradient method. *IEEE Transactions on Signal Processing*, 72:2527–2542, 2024.
- Xiang, R., Xie, J., and Zhang, Q. Randomized block Kaczmarz with volume sampling: Momentum acceleration and efficient implementation. *arXiv preprint arXiv:2503.13941*, 2025.
- Yang, M., Xu, D., Wen, Z., Chen, M., and Xu, P. Sketchy empirical natural gradient methods for deep learning. *arXiv preprint arXiv:2006.05924*, 2020.

A. Proof of Lemma 4.1

Lemma A.1 (Key expectation formula under SVS). *Let $J \in \mathbb{R}^{m \times n}$ with rank e and full SVD $\mathbf{U}\Sigma\mathbf{V}^\top$, and suppose $S \sim \text{SVS}(J, k, \lambda)$. Then*

$$\bar{W} = \mathbb{E}_S [I_S^\top (J_S J_S^\top + \lambda I)^+ I_S] = \mathbf{U}\mathbf{D}\mathbf{U}^\top \quad (27)$$

where

$$\mathbf{D} = \frac{\text{diag}(p_{k-1}(q_{-1}), \dots, p_{k-1}(q_{-m}))}{p_k(q)}, \quad (28)$$

with q the vector of descending eigenvalues of $JJ^\top + \lambda I$ ($q_i = \sigma_i^2 + \lambda$ when $i \leq e$, $q_i = \lambda$ when $i > e$), q_{-i} the vector q with the i^{th} entry removed, and p_i the real elementary symmetric polynomial of degree i .

Proof. See eq. (5.2) of (Dereziński & Yang, 2024). □

Lemma A.2 (Alternative characterization of \tilde{W}). *Let e be the rank of J and let $U\Sigma V^\top$ be its compact SVD. Fix k and λ and define $\tilde{W} = (J^\top J)^{-1/2} \bar{P} (J^\top J)^{-1/2}$ as in Lemma 4.1. Then it holds*

$$\tilde{W} = \mathbf{V}\mathbf{D}\mathbf{V}^\top \quad (29)$$

where $\mathbf{D} = \mathbf{D}[1 : e, 1 : e]$. It also holds $\lambda_{\min}(\mathbf{D}) \geq 1/\text{Tr}(JJ^\top + \lambda I)$.

Proof. First note

$$\bar{P} = \mathbb{E}_S [J_S^{+(\lambda)} J_S] = J^\top \mathbb{E}_S [I_S^\top (J_S J_S^\top + \lambda I)^+ I_S] J = J^\top \bar{W} J. \quad (30)$$

Then substitute

$$\tilde{W} = (J^\top J)^{-1/2} \bar{P} (J^\top J)^{-1/2} = (J^\top J)^{-1/2} J^\top \bar{W} J (J^\top J)^{-1/2} = \mathbf{V}\mathbf{U}^\top (\mathbf{U}\mathbf{D}\mathbf{U}^\top) \mathbf{U}\mathbf{V}^\top = \mathbf{V}\mathbf{D}\mathbf{V}^\top. \quad (31)$$

Finally, using eq. (5.3) of (Dereziński & Yang, 2024) we can lower bound

$$\lambda_{\min}(\mathbf{D}) \geq \min_i \frac{p_{k-1}(q_{-i})}{p_k(q)} \geq \min_i \frac{1}{q_i + \frac{1}{k-1} \sum_{j=2, j \neq i}^m q_j} \geq \frac{1}{q_1 + \frac{1}{k-1} \sum_{j=2}^m q_j} \geq \frac{1}{\sum_{j=1}^m q_j} = \frac{1}{\text{Tr}(JJ^\top + \lambda I)}. \quad (32)$$

This chain of inequalities is ill-defined when $k = 1$ but it is easy to verify that in this case, $p_{k-1}(q_{-i})/p_k(q) = 1/\text{Tr}(JJ^\top + \lambda I)$ for all i and so the bound is still valid. □

Proof of Lemma 4.1. Let e be the rank of J and let $U\Sigma V^\top$ be its compact SVD. Calculate

$$\begin{aligned} \mathbb{E}_S [J_S^{+(\lambda)} r_S] &= \mathbb{E}_S [J_S^\top (J_S J_S^\top + \lambda I)^+ r_S] \\ &= J^\top \mathbb{E}_S [I_S^\top (J_S J_S^\top + \lambda I)^+ I_S] r \\ &= J^\top \mathbf{U}\mathbf{D}\mathbf{U}^\top r \end{aligned}$$

by Lemma A.1. Then, let $\mathbf{D} = \mathbf{D}[1 : e, 1 : e]$ and note also that $\mathbf{U} = \mathbf{U}(:, 1 : e)$ and $\Sigma = \Sigma(1 : e, 1 : e)$. Then we can rewrite

$$\mathbb{E}_S [J_S^{+(\lambda)} r_S] = J^\top \mathbf{U}\mathbf{D}\mathbf{U}^\top r = \mathbf{V}\Sigma\mathbf{U}^\top \mathbf{U}\mathbf{D}\mathbf{U}^\top r = \mathbf{V}\Sigma\mathbf{U}^\top \mathbf{U}\mathbf{D}\mathbf{U}^\top r = \mathbf{V}\Sigma\mathbf{D}\mathbf{U}^\top r = \mathbf{V}\mathbf{D}\Sigma\mathbf{U}^\top r = \mathbf{V}\mathbf{D}\mathbf{V}^\top J^\top r. \quad (33)$$

The result follows since $\tilde{W} = \mathbf{V}\mathbf{D}\mathbf{V}^\top$ by Lemma A.2. □

B. Proofs for Global Convergence of SVS-SNG

Lemma B.1 (Variance of SNG update under SVS). *Let $J \in \mathbb{R}^{m \times n}$, $r \in \mathbb{R}^m$, and $S \sim \text{SVS}(J, k, \lambda)$. Then when $\lambda > 0$ it holds*

$$\mathbb{E}_S \left\| J_S^{+(\lambda)} r_S \right\|^2 \leq \frac{1}{\lambda} \|r\|^2. \quad (34)$$

Proof. Using the push-through identity $J_S^{+(\lambda)} = J_S^\top (J_S J_S^\top + \lambda I)^{-1} = (J_S^\top J_S + \lambda I)^{-1} J_S^\top$ it holds

$$\begin{aligned} \left\| J_S^{+(\lambda)} r_S \right\|^2 &= r_S^\top J_S (J_S^\top J_S + \lambda I)^{-2} J_S^\top r_S \\ &\leq \frac{1}{\lambda} r_S^\top J_S (J_S^\top J_S + \lambda I)^{-1} J_S^\top r_S \\ &\leq \frac{1}{\lambda} \|r_S\|^2 \end{aligned}$$

Hence it follows

$$\mathbb{E}_S \left\| J_S^{+(\lambda)} r_S \right\|^2 \leq \frac{1}{\lambda} \mathbb{E}_S \|r_S\|^2 \leq \frac{1}{\lambda} \mathbb{E}_S \|r\|^2 = \frac{1}{\lambda} \|r\|^2. \quad (35)$$

□

Proof of Theorem 4.2. The result follows directly from (Bottou et al., 2018, Theorem 4.10) once the appropriate conditions are established. The conditions entail some continuity requirements which we have taken as assumptions (Assumption 4.1 in the reference), and some first and second moment limits which we now discuss (Assumption 4.3 in the reference).

The first moment conditions follows straightforwardly from the expectation formula of Lemma 4.1 which states that

$$\mathbb{E}_S \left[J_S^{+(\lambda)} r_S \right] = \tilde{W} J^\top r. \quad (36)$$

Using Lemma A.2 we can rewrite this as

$$\mathbb{E}_S \left[J_S^{+(\lambda)} r_S \right] = V D V^\top J^\top r \quad (37)$$

where $D = \mathbf{D}[1 : e, 1 : e]$ and \mathbf{D} as in (28), and with $\lambda_{\min}(D) \geq 1/\text{Tr}(J J^\top + \lambda I)$. Since $J^\top r = \nabla_\theta \mathcal{L}(v_\theta)$ it follows that

$$\langle \nabla_\theta \mathcal{L}(v_\theta), \mathbb{E}_S \left[J_S^{+(\lambda)} r_S \right] \rangle \geq \frac{1}{\text{Tr}(J J^\top + \lambda I)} \cdot \|\nabla_\theta \mathcal{L}(v_\theta)\|^2. \quad (38)$$

Since we have assumed v_θ is a Lipschitz continuous function of θ , it holds $\|J\|_2 \leq L$ for some constant L and thus $\text{Tr}(J J^\top + \lambda I) \leq nL^2 + m\lambda$, and so condition (4.7a) of the reference is proven. Similarly, regarding (4.7b) we have

$$\left\| \mathbb{E}_S \left[J_S^{+(\lambda)} r_S \right] \right\| = \|V D V^\top J^\top r\| \leq \lambda_{\max}(D) \cdot \|\nabla_\theta \mathcal{L}(v_\theta)\|, \quad (39)$$

and since $\lambda > 0$ by assumption we can upper bound

$$\lambda_{\max}(D) \leq \max_i \frac{p_{k-1}(q-i)}{p_k(q)} \leq \max_i \frac{p_{k-1}(q-i)}{q_i p_{k-1}(q-i) + p_k(q-i)} \leq \frac{1}{q_i} \leq \frac{1}{\lambda}. \quad (40)$$

Finally, regarding the second moment condition we combine the variance bound of Lemma B.1 with the assumption on $\|r\|^2$ to obtain

$$\mathbb{E}_S \left\| J_S^{+(\lambda)} r_S \right\|^2 \leq \frac{1}{\lambda} \|r\|^2 \leq \left(\frac{C_1}{\lambda} \right) \|\nabla_\theta \mathcal{L}(v_\theta)\|^2 + \left(\frac{C_2}{\lambda} \right), \quad (41)$$

which confirms condition (4.8) of the reference. Hence all the assumptions of Theorem 4.10 of (Bottou et al., 2018) are satisfied and the theorem is proven. □

Proposition B.2. *For any fixed instance of LLQ there exist constants C_1, C_2 such that $\|r\|^2 \leq C_1 \|J^\top r\|^2 + C_2$, as required by Theorem 4.2.*

Proof. For any matrix $X \in \mathbb{R}^m$ let $X^{[J]}$ be the orthogonal projection of X to the range of J , namely $UU^\top XU^\top$ where $J = U\Sigma V^\top$ is the compact SVD of J . For LLQ, it holds $r = HJ\theta - b$ and thus we can bound

$$\|r\|^2 = \|HJ\theta - b\|^2 \leq 2\|HJ\theta\|^2 + 2\|b\|^2. \quad (42)$$

The second term is already a constant and so the main task is to bound the first term. To do so note

$$\|HJ\theta\|^2 = \theta^\top J^\top H^2 J \theta = \theta^\top J^\top (H^2)^{[J]} J \theta \leq C \theta^\top J^\top (H^{[J]})^2 J \theta \quad (43)$$

for some constant C , with the last inequality holding since $(H^2)^{[J]}$ and $(H^{[J]})^2$ both define fixed norms on $\text{range}(J)$. It follows that

$$\|HJ\theta\|^2 \leq C \theta^\top J^\top (H^{[J]}) (H^{[J]}) J \theta \leq \frac{C}{\lambda_{\min}^+(JJ^\top)} \theta^\top J^\top H^{[J]} (JJ^\top) H^{[J]} J \theta = \frac{C}{\lambda_{\min}^+(JJ^\top)} \|J^\top HJ\theta\|^2. \quad (44)$$

Finally, $\|J^\top HJ\theta\|^2 = \|J^\top r + J^\top b\|^2 \leq 2\|J^\top r\|^2 + 2\|J^\top b\|^2$, and as a result it suffices to choose

$$C_1 = \frac{4C}{\lambda_{\min}^+(JJ^\top)}, \quad C_2 = 2\|b\|^2 + 4\|J^\top b\|^2. \quad (45)$$

□

C. Proofs for Convergence Rate Analysis of SVS-SNG

Lemma C.1 (Range containment). *If $\theta_0 \in \text{range}(J^\top)$ then $\theta_t \in \text{range}(J^\top)$ for all t .*

Proof. Consider the SNG iteration

$$\theta_{t+1} = \theta_t - \eta J_S^{+(\lambda)} r_S = \theta_t - \eta J^\top I_S^\top (J_S J_S^\top + \lambda I)^+ r_S. \quad (46)$$

Clearly then $\theta_t \in \text{range}(J^\top) \implies \theta_{t+1} \in \text{range}(J^\top)$ and the result follows by induction. □

Proof of Theorem 5.1. For linear least-quadratics the SNG iteration takes the form

$$\theta_{t+1} = \theta_t - \eta J_S^{+(\lambda)} (H_S J \theta_t - b_S). \quad (47)$$

In the consistent case $\nabla_v \mathcal{L}(v_{\theta^*}) = 0 \implies HJ\theta^* = b$ so we can rewrite this iteration as

$$\theta_{t+1} - \theta^* = (I - \eta J_S^{+(\lambda)} H_S J) (\theta_t - \theta^*). \quad (48)$$

Now, note that since Lemma 4.1 holds for arbitrary r it can be applied separately to each column of HJ to show that

$$\mathbb{E}_S \left[J_S^{+(\lambda)} H_S J \right] = \tilde{W} J^\top H J. \quad (49)$$

Note also that although \tilde{W} is not necessarily full rank on the entirety of \mathbb{R}^n , Lemma A.2 shows that it is full rank and positive definite when restricted to $\text{range}(J^\top) = \text{range}(V)$, which contains all the iterates θ_t by Lemma C.1. As a result we can meaningfully measure the solution error by $\|\theta - \theta^*\|_{\tilde{W}^+}^2 = (\theta - \theta^*)^\top \tilde{W}^+ (\theta - \theta^*)$. Using this technique to cancel out the factors of \tilde{W} in the cross-terms, we find

$$\mathbb{E} \|\theta_{t+1} - \theta^*\|_{\tilde{W}^+}^2 = (\theta_t - \theta^*)^\top \left(\tilde{W}^+ - 2\eta J^\top H J + \eta^2 J^\top H \mathbb{E}_S \left[I_S^\top (J_S^{+(\lambda)})^\top \tilde{W}^+ J_S^{+(\lambda)} I_S \right] H J \right) (\theta_t - \theta^*). \quad (50)$$

Using the definition of γ it follows

$$\begin{aligned} \mathbb{E} \|\theta_{t+1} - \theta^*\|_{\tilde{W}^+}^2 &\leq (\theta_t - \theta^*)^\top \left(\tilde{W}^+ - 2\eta J^\top H J + \eta^2 \gamma \cdot J^\top H^2 J \right) (\theta_t - \theta^*) \\ &\leq (\theta_t - \theta^*)^\top \left(\tilde{W}^+ - 2\eta J^\top H J + \eta \gamma \|H\|_2 \cdot \eta J^\top H J \right) (\theta_t - \theta^*). \end{aligned}$$

Hence when $\eta \leq 1/(\gamma\|H\|_2)$ we obtain

$$\begin{aligned} \mathbb{E} \|\theta_{t+1} - \theta^*\|_{\tilde{W}^+}^2 &\leq (\theta_t - \theta^*)^\top \left(\tilde{W}^+ - \eta J^\top H J \right) (\theta_t - \theta^*) \\ &\leq (\theta_t - \theta^*)^\top \left(\tilde{W}^+ - \eta \cdot \lambda_{\min}(H) \cdot J^\top J \right) (\theta_t - \theta^*). \end{aligned}$$

Furthermore by the definition of \tilde{W} it holds

$$\tilde{W}^+ = (J^\top J)^{1/2} \bar{P}^+ (J^\top J)^{1/2} \preceq \frac{1}{\alpha} (J^\top J), \quad (51)$$

and substituting this inequality into the above bound yields

$$\mathbb{E} \|\theta_{t+1} - \theta^*\|_{\tilde{W}^+}^2 \leq (\theta_t - \theta^*)^\top ([1 - \eta \cdot \lambda_{\min}(H) \cdot \alpha] \tilde{W}^+) (\theta_t - \theta^*) = (1 - \eta \cdot \lambda_{\min}(H) \cdot \alpha) \|\theta_t - \theta^*\|_{\tilde{W}^+}^2. \quad (52)$$

Finally, iterating this bound yields the theorem. \square

Proof of Corollary 5.2. We can recover the desired deterministic natural gradient descent from SNG by setting $k = m$ and $\lambda = 0$. In this case, the same proof as in Proposition 5.3 shows that $\gamma = 1$. Additionally it holds that $\bar{P} = J^+ J$ is a projector matrix. This implies that $\alpha = \lambda_{\min}^+(\bar{P}) = 1$, and it also implies that

$$\tilde{W} = (J^\top J)^{-1/2} \bar{P} (J^\top J)^{-1/2} = (J^\top J)^+. \quad (53)$$

Substituting these values into Theorem 5.1 yields the corollary. \square

Proof of Proposition 5.3. Consider first the case when $\lambda = 0$ and $S \sim \text{SVS}(J, k, \lambda)$. Under this assumption recall the definition

$$\gamma = \left\| \mathbb{E}_S \left[I_S^\top (J_S^+)^{\top} \tilde{W}^+ J_S^+ I_S \right] \right\|. \quad (54)$$

Within this context, consider first the case when $k = 1$. In this case the sampling distribution simplifies to $p(i) = \|J_i\|^2 / \|J\|_F^2$ and it holds

$$\bar{P} = \mathbb{E}_i \left[\frac{J_i^\top J_i}{\|J_i\|^2} \right] = \frac{1}{\|J\|_F^2} \sum_{i=1}^m J_i^\top J_i = \frac{J^\top J}{\|J\|_F^2}. \quad (55)$$

It follows that $\tilde{W} = (J^\top J)^{-1/2} \bar{P} (J^\top J)^{-1/2} = \frac{1}{\|J\|_F^2} \Pi_J$ where Π_J is the projector onto $\text{range}(J^\top)$. Thus

$$\mathbb{E}_i \left[I_i^\top (J_i^+)^{\top} \tilde{W}^+ J_i^+ I_i \right] = \|J\|_F^2 \mathbb{E}_i \left[\frac{I_i^\top I_i}{\|J_i\|^2} \right] = \sum_{i=1}^m I_i^\top I_i = I, \quad (56)$$

and it follows that $\gamma = 1$.

Consider next the case that $k = m$. In this case there is no stochasticity and so

$$\bar{P} = \mathbb{E}_S [J_S^+ J_S] = J^+ J = V V^\top \implies \tilde{W} = (J^\top J)^{-1}, \quad (57)$$

where $U \Sigma V^\top$ is the compact SVD of J . Furthermore

$$\mathbb{E}_S \left[I_S^\top (J_S^+)^{\top} \tilde{W}^+ J_S^+ I_S \right] = (J^+)^{\top} \tilde{W}^+ J^+ = (J J^+)^{\top} J J^+ = U U^\top \quad (58)$$

and so again it follows that $\gamma = 1$.

We now turn our attention to the upper bound on γ which holds when $\lambda > 0$ and the sampling is uniform. As a start note that in this case, \bar{W} is full rank since

$$\bar{W} = \mathbb{E}_S \left[I_S^\top (J_S J_S^\top + \lambda I)^{-1} I_S \right] \succeq \frac{1}{C} \mathbb{E}_S [I_S^\top I_S] = \frac{k}{mC} I \succ 0 \quad (59)$$

where $C = \max_S \|J_S J_S^\top + \lambda I\|_2$. Note also that by the definition of \tilde{W} it holds

$$\tilde{W} = (J^\top J)^{-1/2} J^\top \bar{W} J (J^\top J)^{-1/2} = V U^\top \bar{W} U V^\top \quad (60)$$

where $U \Sigma V^\top$ is the compact SVD of J . Using the Rayleigh-Ritz variational principle and the fact that V and U have orthonormal columns it follows that

$$\lambda_{\min}^+(\tilde{W}) = \min_{\substack{u \in \text{range}(V) \\ \|u\|=1}} u^\top V U^\top \bar{W} U V^\top u = \min_{\substack{u \in \mathbb{R}^{\text{rank}(J)} \\ \|u\|=1}} u^\top U^\top \bar{W} U u \geq \min_{\substack{u \in \mathbb{R}^m \\ \|u\|=1}} u^\top \bar{W} u = \lambda_{\min}(\bar{W}), \quad (61)$$

from which we can conclude that

$$\|\tilde{W}^+\|_2 \leq \|\bar{W}^{-1}\|_2. \quad (62)$$

We can thus calculate

$$\begin{aligned} \gamma &= \left\| \mathbb{E}_S \left[I_S^\top (J_S^{+(\lambda)})^\top \tilde{W}^+ J_S^{+(\lambda)} I_S \right] \right\|_2 \\ &\leq \|\bar{W}^{-1}\|_2 \cdot \left\| \mathbb{E}_S \left[I_S^\top (J_S^{+(\lambda)})^\top J_S^{+(\lambda)} I_S \right] \right\|_2 \\ &= \|\bar{W}^{-1}\|_2 \cdot \left\| \mathbb{E}_S \left[I_S^\top (J_S J_S^\top + \lambda I)^+ J_S J_S^\top (J_S J_S^\top + \lambda I)^+ I_S \right] \right\|_2 \\ &\leq \|\bar{W}^{-1}\|_2 \cdot \left\| \mathbb{E}_S \left[I_S^\top (J_S J_S^\top + \lambda I)^+ I_S \right] \right\|_2 \\ &= \|\bar{W}^{-1}\|_2 \cdot \|\bar{W}\|_2 \\ &= \kappa(\bar{W}). \end{aligned}$$

Invoking Theorem 5.1 of (Goldshlager et al., 2025) then yields the desired bound. \square

Lemma C.2 (Projected Hessian). *Let $H \succ 0$, assume $[H, J J^\top] = 0$, and define $\tilde{H} = J^+ H J$. It follows that*

$$\tilde{H} = V \Lambda V^\top \quad (63)$$

where $U \Sigma V^\top$ is the compact SVD of J and Λ is diagonal with $\lambda_{\min}(H) \leq \lambda_{\min}(\Lambda) \leq \lambda_{\max}(\Lambda) \leq \lambda_{\max}(H)$.

Proof. By the assumptions $H \succ 0$ and $[H, J J^\top] = 0$, H admits an orthogonal decomposition $H = U \Lambda U^\top + H_\perp$ where $\Lambda \succ 0$ is diagonal, $H_\perp \succ 0$ and $J^\top H_\perp = H_\perp J = 0$. It follows that

$$\tilde{H} = J^+ H J = V \Lambda V^\top. \quad (64)$$

Furthermore, the eigenvalues of Λ are a subset of the eigenvalues of H due to the orthogonal decomposition and are thus contained within $[\lambda_{\min}(H), \lambda_{\max}(H)]$. \square

Lemma C.3 (Expected projection). *Let $S \sim \text{SVS}(J, k, \lambda)$ and define $\alpha = \lambda_{\min}^+(\bar{P})$, $\bar{P} = \mathbb{E}_S [P(S)]$, $P(S) = J_S^{+(\lambda)} J_S$. It follows that*

$$\bar{P} = V \Lambda V^\top \quad (65)$$

where $U \Sigma V^\top$ is the compact SVD of J and $\Lambda \succeq \alpha I$ is diagonal.

Proof. Using Lemma A.1 and defining $D = \mathbf{D}[1 : e, 1 : e]$ we have

$$\begin{aligned} \bar{P} &= \mathbb{E}_S \left[J_S^{+(\lambda)} J_S \right] \\ &= J^\top \mathbb{E}_S \left[I_S^\top (J_S J_S^\top + \lambda I)^+ I_S \right] J \\ &= J^\top \mathbf{U} \mathbf{D} \mathbf{U}^\top J \\ &= V (\Sigma U^\top \mathbf{U} \mathbf{D} \mathbf{U}^\top U \Sigma) V^\top \\ &= V (\Sigma D \Sigma) V^\top. \end{aligned}$$

The result follows by defining $\Lambda = \Sigma D \Sigma$. \square

Proof of Proposition 5.4. To start define $\tilde{H} = J^+ H J$ and let $U \Sigma V^\top$ be the compact SVD of J . For linear least-quadratics the SNG iteration takes the form

$$\theta_{t+1} = \theta_t - \eta J_S^{+(\lambda)} (H_S J \theta_t - b_S). \quad (66)$$

In the consistent case $\nabla_v \mathcal{L}(v_{\theta^*}) = 0 \implies H J \theta^* = b$ so we can rewrite this iteration as

$$\theta_{t+1} - \theta^* = (I - \eta J_S^{+(\lambda)} H_S J) (\theta_t - \theta^*). \quad (67)$$

Using the assumption $[H, J J^\top] = 0$ it holds $\text{range}(H J) = \text{range}(J)$ and thus

$$H_S J = I_S H J = I_S J J^+ H J = J_S \tilde{H}. \quad (68)$$

This leads to the equivalent form

$$\theta_{t+1} - \theta^* = (I - \eta J_S^{+(\lambda)} J_S \tilde{H}) (\theta_t - \theta^*) = (I - \eta P(S) \tilde{H}) (\theta_t - \theta^*). \quad (69)$$

Taking squared norms and then expectations we obtain

$$\begin{aligned} \mathbb{E} \|\theta_{t+1} - \theta^*\|^2 &= (\theta_t - \theta^*)^\top \left(I - 2\eta \bar{P} \tilde{H} + \eta^2 \tilde{H} \mathbb{E}_S [P(S)^2] \tilde{H} \right) (\theta_t - \theta^*) \\ &\leq (\theta_t - \theta^*)^\top \left(I - 2\eta \bar{P} \tilde{H} + \eta^2 \tilde{H} \bar{P} \tilde{H} \right) (\theta_t - \theta^*) \end{aligned}$$

using $P(S) \preceq I \implies P(S)^2 \preceq P(S)$. Now, using Lemmas C.2 and C.3 we see that \bar{P} commutes with \tilde{H} and thus when $\eta \leq 1/\|\tilde{H}\|_2$ it holds $\eta^2 \tilde{H} \bar{P} \tilde{H} \preceq \eta \bar{P} \tilde{H}$, leading to the simpler bound

$$\mathbb{E} \|\theta_{t+1} - \theta^*\|^2 \leq (\theta_t - \theta^*)^\top \left(I - \eta \bar{P} \tilde{H} \right) (\theta_t - \theta^*). \quad (70)$$

Again applying Lemmas C.2 and C.3 to write $\bar{P} = V \Lambda_P V^\top$, $\tilde{H} = V \Lambda_H V^\top$ we have

$$\mathbb{E} \|\theta_{t+1} - \theta^*\|^2 \leq (\theta_t - \theta^*)^\top \left(I - \eta V \Lambda_P \Lambda_H V^\top \right) (\theta_t - \theta^*). \quad (71)$$

By Lemma C.1 it holds $\theta_t - \theta^* \in \text{range}(V)$ and thus

$$\mathbb{E} \|\theta_{t+1} - \theta^*\|^2 \leq (1 - \eta \cdot \lambda_{\min}(\Lambda_P) \cdot \lambda_{\min}(\Lambda_H)) \|\theta_t - \theta^*\|^2. \quad (72)$$

Using $\lambda_{\min}(\Lambda_P) \geq \alpha$, $\lambda_{\min}(\Lambda_H) \geq \lambda_{\min}(H)$ it follows

$$\mathbb{E} \|\theta_{t+1} - \theta^*\|^2 \leq (1 - \eta \cdot \lambda_{\min}(H) \cdot \alpha) \|\theta_t - \theta^*\|^2, \quad (73)$$

and iterating this bound yields the proposition. \square

D. Proof for SPRING as an Accelerated Sketch-and-Project Method

Proof of Theorem 6.1. The recent work of (Dereziński et al., 2025b) was the first to incorporate regularization into an accelerated sketch-and-project algorithm. That work focused on the case of randomized block Kaczmarz methods but their formulation extends trivially to general sketch-and-project algorithms. In this more general context their method takes the form

$$\begin{aligned} w_t &= (\Omega_t J)^{+(\lambda)} (\Omega_t J \tilde{\theta}_t - \Omega_t b), \\ \tilde{\phi}_{t+1} &= \mu (\tilde{\phi}_t - w_t), \\ \tilde{\theta}_{t+1} &= \tilde{\theta}_t - w_t + \tilde{\eta} \tilde{\phi}_{t+1}. \end{aligned} \quad (74)$$

We use the symbols $\tilde{\theta}$, $\tilde{\phi}$, $\tilde{\eta}$ since these variables do not correspond directly to the variables θ , ϕ , η of our formulation. We also recall for convenience the formulation that we have proposed, recalling from equation (22) the following iteration:

$$\begin{aligned} \phi_{t+1} &= \mu \phi_t + (\Omega_t J)^{+(\lambda)} (\Omega_t b - \Omega_t J (\theta_t + \mu \phi_t)), \\ \theta_{t+1} &= \theta_t + \eta \phi_{t+1}. \end{aligned} \quad (75)$$

We next show that the algorithm of equation (75) with initial guess θ_0 , initial momentum $\phi_0 = 0$, momentum coefficient μ , and step size η is equivalent to the algorithm of equation (74) with initial guess $\tilde{\theta}_0 = \theta_0$, initial momentum $\tilde{\phi}_0 = 0$, momentum coefficient μ , and step size $\tilde{\eta} = 1 - \frac{1-\eta}{\mu}$ in that the resulting iterates satisfy $\tilde{\phi}_t = \mu\phi_t$, $\tilde{\theta}_t = \theta_t + \mu\phi_t$.

Proceeding by induction, as a base case we have $\tilde{\phi}_0 = \mu\phi_0 = 0$ and $\tilde{\theta}_0 = \theta_0 + \mu\phi_0 = \theta_0$. Now, suppose these identities hold for some fixed $t \geq 0$. Then calculate using (74) and (75)

$$\begin{aligned}\tilde{\phi}_{t+1} &= \mu(\tilde{\phi}_t - (\Omega_t J)^{+(\lambda)}(\Omega_t J \tilde{\theta}_t - \Omega_t b)) \\ &= \mu(\mu\phi_t - (\Omega_t J)^{+(\lambda)}(\Omega_t J(\theta_t + \mu\phi_t) - \Omega_t b)) \\ &= \mu(\mu\phi_t + (\Omega_t J)^{+(\lambda)}(\Omega_t b - \Omega_t J(\theta_t + \mu\phi_t))) \\ &= \mu\phi_{t+1}.\end{aligned}$$

Using the above, proceed to verify

$$\begin{aligned}\tilde{\theta}_{t+1} &= \tilde{\theta}_t - (\Omega_t J)^{+(\lambda)}(\Omega_t J \tilde{\theta}_t - \Omega_t b) + \tilde{\eta} \tilde{\phi}_{t+1} \\ &= \theta_t + \mu\phi_t - (\Omega_t J)^{+(\lambda)}(\Omega_t J(\theta_t + \mu\phi_t) - \Omega_t b) + \left(1 - \frac{1-\eta}{\mu}\right) \mu\phi_{t+1} \\ &= \theta_t + \phi_{t+1} + \mu\phi_{t+1} - (1-\eta)\phi_{t+1} \\ &= (\theta_t + \eta\phi_{t+1}) + \mu\phi_{t+1} \\ &= \theta_{t+1} + \mu\phi_{t+1}.\end{aligned}$$

This completes the inductive step.

We now turn our attention to the SPRING algorithm. In particular we consider applying the new accelerated sketch-and-project step of equation (75) to the natural gradient subproblem (3) with the row sampling sketching matrix I_S . We should be careful about the step sizes here since as defined, both the natural gradient subproblem *and* the accelerated sketch-and-project step have step size parameters. As such let us use the notation η_1 to denote the step size of the subproblem and η_2 to denote the step size of the accelerated sketch-and-project step. We then obtain the update formulas

$$\begin{aligned}\phi_{t+1} &= \mu\phi_t + J_S^{+(\lambda)}((-\eta_1 r + J\theta_t)_S - J_S(\theta_t + \mu\phi_t)) \\ &= \mu\phi_t + J_S^{+(\lambda)}(-\eta_1 r_S - \mu J_S \phi_t), \\ \theta_{t+1} &= \theta_t + \eta_2 \phi_{t+1}.\end{aligned}\tag{76}$$

Rescaling $\phi \leftarrow -\phi/\eta_1$ we can rewrite this as

$$\begin{aligned}\phi_{t+1} &= \mu\phi_t + J_S^{+(\lambda)}(r_S - \mu J_S \phi_t), \\ \theta_{t+1} &= \theta_t - \eta_1 \eta_2 \phi_{t+1}.\end{aligned}\tag{77}$$

Finally, joining the step sizes using $\eta = \eta_1 \eta_2$ yields the standard form of SPRING:

$$\begin{aligned}\phi_{t+1} &= \mu\phi_t + J_S^{+(\lambda)}(r_S - \mu J_S \phi_t), \\ \theta_{t+1} &= \theta_t - \eta \phi_{t+1}.\end{aligned}\tag{78}$$

□

E. Ablation for Figure 2: Non-Gaussian Data

In this section we provide a simple ablation study to show that the suitability of SVS-SNG as a theoretical proxy for realistic SNG algorithms is not limited to strictly Gaussian data scenarios. To do so, we re-run the experiments of Figure 2 with the same data matrices but with a single row of the Jacobian inflated by a factor of 100 in order to break the Gaussian structure. The results in Figure 6 show that even with this adversarial row insertion, SVS-SNG is still a much better proxy for the realistic SNG algorithm than the previously studied algorithm with two independent mini-batches. Interestingly, the only regime in which the row insertion meaningfully affects the quality of SVS as a proxy is in the case of very small values of the regularization parameter λ . On the other hand, the row insertion completely breaks the two mini-batch algorithm which is now unable to make progress in reducing the solution error under any of the tested hyperparameter settings.

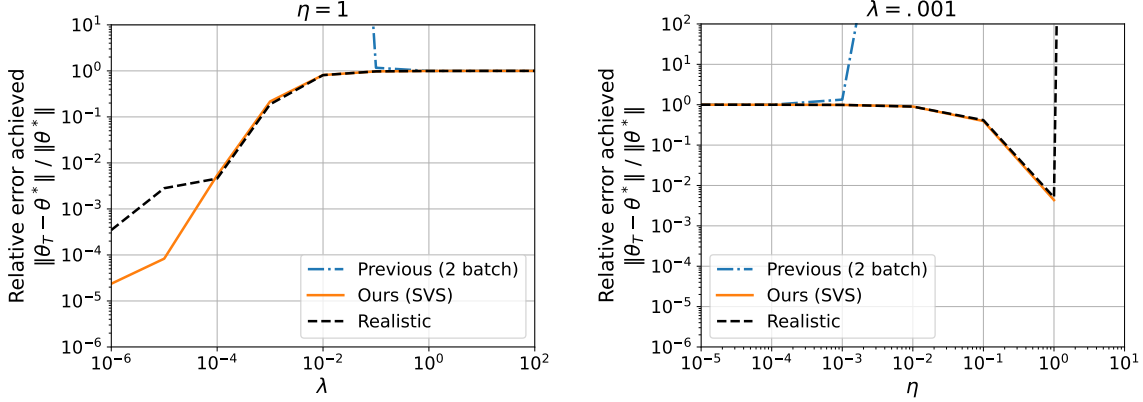


Figure 6. Empirical performance of two theoretical models for SNG relative to a realistic algorithm using a single, uniformly sampled mini-batch. The results are for consistent instances of linear least-quadratics, the Jacobian J is a random Gaussian matrix with its first row inflated by a factor of 100, and the behavior is tested for fixed η and varying λ (left) as well as fixed λ and varying η (right). In both cases the behavior of SVS-SNG matches qualitatively with the behavior of the realistic algorithm, while the behavior of the previously studied algorithm with two independent mini-batches is entirely distinct. The dimensions are $m = 10^3$, $n = 10^2$, and $k = 10$, which is small enough to directly implement SVS. The y -axis represents the relative error achieved after $T = 10^3$ iterations.

F. Details of Numerical Experiments

In this appendix we provide the details for our numerical experiments. The code is attached in the supplementary information.

F.1. Figures 2 and 6

For both Figures 2 and 6 J is initially constructed with independent standard normal entries. For Figure 6 only, the first row of J is then multiplied by 100 to introduce some hidden structure which can be adversarial for the case of uniform sampling. Finally, in both cases the matrix J is normalized to have a maximum singular value of 1.

For both Figures 2 and 6 the H matrix is constructed as

$$H = LL^\top / \|LL^\top\|_2 \quad (79)$$

where L is an $m \times m$ matrix with standard random normal entries. The solution θ^* is then also constructed with standard random normal entries and the linear term of the loss is constructed as $b = HJ\theta^*$ to ensure consistency.

F.2. Figure 3

For Figure 3 J is the only matrix that must be instantiated, and it is constructed as

$$J = Q_1 D Q_2 \quad (80)$$

where Q_1 is a random $m \times n$ matrix with orthonormal columns, D is a diagonal matrix with $D_{ii} = 1/i^2$, and Q_2 is a random $n \times n$ orthogonal matrix. Given J and assuming SVS, we can compute \bar{P} directly using elementary symmetric polynomials; see for example the proof of Lemma C.3. This enables a direct computation of α as well. For γ , we draw samples from $\text{SVS}(J, k, \lambda)$ to estimate the required matrix

$$X = \mathbb{E}_S \left[I_S^\top (J_S^{+(\lambda)})^\top \tilde{W}^+ J_S^{+(\lambda)} I_S \right], \quad (81)$$

and we then directly compute the norm of X . To provide a reasonable estimation of X across all sample sizes, we allocated an equal time budget of five minutes for each value of k , which resulted in sample counts [23503, 24946, 20586, 21017, 6610], respectively. For $k = 1$ we already know that $\gamma = 1$ by Proposition 5.3 so we simply plot this value without any sampling.

F.3. Figure 4

For Figure 4 the Jacobian is constructed as

$$J = Q_1 D Q_2 \quad (82)$$

where Q_1 is a random $m \times n$ matrix with orthonormal columns, D is a diagonal matrix with $D_{ii} = 1/i^2$, and Q_2 is a random $n \times n$ orthogonal matrix. For the inset the set-up is the same except that $D = I$. The quantities H, θ^*, b are constructed exactly as for Figures 2 and 6 (see for example (79)). To estimate the convergence rate for each value of k we fit a linear function to the logarithm of the solution errors ($\|\theta_0 - \theta^*\|^2, \|\theta_1 - \theta^*\|^2, \dots, \|\theta_T - \theta^*\|^2$) and use the slope of the fit as an estimate for the empirical convergence rate.

E.4. Figure 5

For Figure 5 we construct

$$J = Q_1 D Q_2 \tag{83}$$

where Q_1 is a random $m \times n$ matrix with orthonormal columns, D is a diagonal matrix with $D_{ii} = 1/i$, and Q_2 is a random $n \times n$ orthogonal matrix. We further construct

$$H = Q D Q^\top \tag{84}$$

where Q is a random $m \times m$ orthogonal matrix and D is a diagonal $m \times m$ matrix with

$$D_{ii} = \frac{1}{1 + (i-1) \cdot \frac{n-1}{m-1}} \tag{85}$$

so that $D_{11} = 1$, $D_{mm} = 1/n$, and $\kappa(H) = n = 100$. From there the values of θ^* and b are constructed as in the other experiments (θ random normal, b for consistency).

To tune η for SNG we use a dynamic grid search starting from $\eta = 1$ and exploring values on a logarithmic grid ($\eta = 2^i$ for various integers i) until we find a value that performs better than any other value within 2 grid steps. Similarly for SPRING we tune η and μ by starting at $\eta = 1, \mu = 0$ and exploring values on a logarithmic grid ($\eta = 2^i, \mu = 1 - 2^{-j}$ for various integers i and nonnegative integers j) until we find a value that performs better than any other value within at most 2 grid steps in each dimension. Once the optimal hyperparameters are found, the empirical rate constants are measured in the same way as for Figure 4.

Disclaimer

This report was prepared as an account of work sponsored by an agency of the United States Government. Neither the United States Government nor any agency thereof, nor any of their employees, makes any warranty, express or implied, or assumes any legal liability or responsibility for the accuracy, completeness, or usefulness of any information, apparatus, product, or process disclosed, or represents that its use would not infringe privately owned rights. Reference herein to any specific commercial product, process, or service by trade name, trademark, manufacturer, or otherwise does not necessarily constitute or imply its endorsement, recommendation, or favoring by the United States Government or any agency thereof. The views and opinions of authors expressed herein do not necessarily state or reflect those of the United States Government or any agency thereof.